Paraxial speckle-based metrology systems with an aperture

Damien P. Kelly, Jennifer E. Ward, Bryan M. Hennelly, Unnikrishnan Gopinathan, Feidhlim T. O'Neill, and John T. Sheridan

School of Electrical, Electronic and Mechanical Engineering, College of Engineering, Mathematical and Physical Sciences, University College Dublin, Belfield, Dublin 4, Ireland

Received February 10, 2006; revised May 11, 2006; accepted May 16, 2006; posted June 14, 2006 (Doc. ID 67900)

Digital speckle photography can be used in the analysis of surface motion in combination with an optical linear canonical transform (LCT). Previously [D. P. Kelly *et al.* Appl. Opt. **44**, 2720 (2005)] it has been shown that optical fractional Fourier transforms (OFRTs) can be used to vary the range and sensitivity of speckle-based metrology systems, allowing the measurement of both the magnitude and direction of tilting (rotation) and translation motion simultaneously, provided that the motion is captured in two separate OFRT domains. This requires two bulk optical systems. We extend the OFRT analysis to more general LCT systems with a single limiting aperture. The effect of a limiting aperture in LCT systems is examined in more detail by deriving a generalized Yamaguchi correlation factor. We demonstrate the benefits of using an LCT approach to metrology design. Using this technique, we show that by varying the curvature of the illuminating field, we can effectively change the output domain. From a practical perspective this means that estimation of the motion of a target can be achieved by using one bulk optical system and different illuminating conditions. Experimental results are provided to support our theoretical analysis.

OCIS codes: 120.6150, 070.0070, 120.3940, 070.6020.

1. INTRODUCTION

Digital speckle photography is a well-known technique in speckle metrology.[1–20] An optically rough target is illuminated with coherent light, and the speckle field produced by the target, before and after, motion or deformation[1–20] is captured, using a CCD camera. In some cases the speckle field is first manipulated by some optical signal processing (OSP) system before capture. For example, Tiziani,[11] demonstrated that by passing the reflected speckle field though a bulk optical Fourier transform (OFT) system, accurate measurement of small surface tilts of an optically rough target could be achieved. This metrology system is sometimes simply referred to as a defocused system[11,15]

Other OSP systems besides the OFT arrangement just mentioned can be used, and we discuss some of these now. The fractional Fourier transform (FRT) describes wave propagation in graded-index media[21–29] and can also be implemented by using bulk optics.[27,28] Briefly, the FRT order indicates the domain into which a given function is transformed, and an order of $a=1$ is simply the Fourier transform (FT). The FRT angle θ is related to the FRT order by $\theta=a(\pi/2)$. Sheridan *et al.*[16,17] showed that an optical FRT (OFRT) system could be used, in a manner similar to that of Tiziani,[11] to vary the sensitivity of the metrology system to both tilting and translation motion by varying the fractional angle associated with the OFRT. Later, using a geometric interpretation based on the use of the Wigner distribution function (WDF),[21,29,30] it was shown[18] that by projecting the motion (both tilting and translation) of the rigid body onto two different OFRT domains, i.e., passing the reflected speckle field through two OFRT systems of different order, information about both the tilting and in-plane translation could be extracted. This theoretical prediction was also experimentally verified.[19,20] Widjaja *et al.*[31] demonstrated that, by optically generating the WDF, information about local displacement of objects could be extracted by examining localized spatial and spatial-frequency distributions of the reflected speckle field.

The linear canonical transform (LCT) can be used to model quadratic phase systems (QPSs), which include as special cases the OFT, OFRT, the Fresnel transform (FST), and the effect of a thin lens or chirp modulation transform (CMT).[21,29,32] To measure both tilting and translation motion for an OFRT-based metrology system, projection of the motion onto two different separated OFRT domains is necessary.[18] This is also the case for an LCT-based system, and thus typically two optical systems and two CCD cameras are required to unambiguously determine the motions. There are, however, distinct advantages to using an LCT system such as increased design flexibility.

The layout for the rest of the paper is as follows: In Section 2.A we derive a generalized Yamaguchi correlation factor for an arbitrary LCT system. In Section 2.B we examine some of the advantages of an LCT-based analysis in the design of metrology systems. In Section 2.C we show that by varying the curvature of the illuminating field, we can change the LCT domain, allowing simultaneous translation and tilt motion to be measured unambiguously. In Section 3 we provide experimental results, which support our theoretical analysis.

2. THEORETICAL ANALYSIS

In this section we examine three separate issues. In Subsection 2.A we derive a generalized Yamaguchi correlation

factor, and show that an LCT-based analysis is a useful means for estimating the in-plane translation and tilting motion of a rough surface. In Subsection 2.B we show that by using an LCT approach, it is possible to analyze, optimize, and design metrology systems. Finally, in Subsection 2.C we examine the effect of varying the curvature of the illuminating field on the characteristics of the metrology system.

A. Linear Canonical Transform Metrology Systems with Limiting Aperture

The purpose of this subsection is to derive some important properties of general bulk optical systems. We describe the complete metrology system by using two separate LCTs as in Fig. 1. The first LCT describes the field incident on the aperture, and the second describes the propagation of the field from the aperture to the camera plane. We assume that any optical elements, e.g., lens, are infinite in extent and attribute any losses in the system to the single limiting aperture (see Fig. 1). In Fig. 1, $u(x_0)$ represents the speckle field at the optically rough surface. If the optically rough surface is translated by an amount ξ and rotated through an angle α, then the altered field may be represented by[15,18–20]

$$\tilde{u}(\tilde{x}_0) = u(x_0 + \xi)\exp\left(j\frac{2\pi}{\lambda}\kappa x_0\right), \tag{1}$$

where $\kappa \sim 2\alpha$ if $\alpha \ll 1$ rad.

The field $u_a(x_a)$ incident on the aperture prior to motion can be found by applying an LCT to $u(x_0)$ (see Fig. 1). Using Ref. 32, we define and apply a one-dimensional (1-D) LCT to the field $u(x_0)$ to give

$$u_a(x_a) = \left(\frac{1}{\sqrt{j\lambda B_1}}\right)\int_{-\infty}^{\infty} u(x_0)\exp\left[\frac{j\pi}{\lambda B_1}(D_1 x_a^2 + A_1 x_0^2 - 2x_a x_0)\right]\mathrm{d}x_0, \tag{2a}$$

$$\begin{pmatrix} x_a \\ k_a \end{pmatrix} = \begin{bmatrix} A_1 & B_1 \\ C_1 & D_1 \end{bmatrix}\begin{pmatrix} x_0 \\ k_0 \end{pmatrix}, \tag{2b}$$

where x_a indicates the domain into which the function $u(x_0)$ is transformed and λ is the wavelength of the illuminating light. We drop the term in the round brackets above from now on. The effect of this integral transform in mapping between the input signal (spatial coordinate x_0, spatial-frequency coordinate k_0) and output signal (x_a, k_a) coordinate systems can be described by using the *ABCD* matrix notation of Collins.[33] In this matrix, $A_1D_1 - B_1C_1 = 1$, indicating a lossless affine transformation. It is important to note that the signal $u_a(x_a)$ is in general in a mixed spatial–spatial-frequency domain.[34]

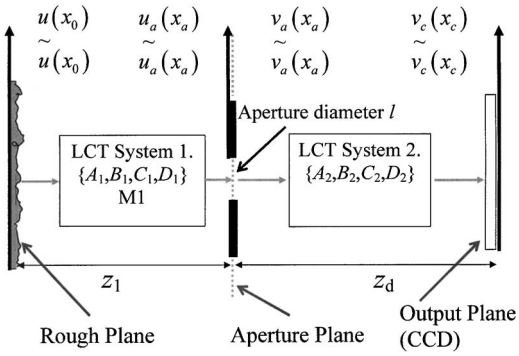

Fig. 1. Optical arrangement for a speckle-photography-based metrology system.

Similarly the field incident on the aperture after motion is given by

$$\tilde{u}_a(\tilde{x}_a) = \int \tilde{u}(\tilde{x}_0)\exp\left[\frac{j\pi}{\lambda B_1}(D_1\tilde{x}_a^2 + A_1\tilde{x}_0^2 - 2\tilde{x}_a\tilde{x}_0)\right]\mathrm{d}\tilde{x}_0, \tag{3a}$$

which may also be written as a shifted version of the LCT of the original field[32,35]:

$$\tilde{u}_a(\tilde{x}_a) = u_a(x_a + \xi_a)\exp(j2\pi\kappa_a x_a/\lambda), \tag{3b}$$

where $\xi_a = A_1\xi + B_1\kappa$ and $\kappa_a = C_1\xi + D_1\kappa$. We have dropped a constant phase factor in the above expression and will continue to do so for the rest of the analysis. From Eq. (3b) we can see that $u_a(x_a)$ and $\tilde{u}_a(\tilde{x}_a)$ are identical apart from a spatial shift and a linear phase term.[32,35]

The fields $v_a(\cdot)$ and $\tilde{v}_a(\cdot)$ immediately after the aperture, prior to and following motion, respectively, are not the same, as the aperture ensures that some spatial and spatial-frequency information is eliminated and some "new information" introduced (see Fig. 1). As the surface in the input plane is moved or deformed, a CCD camera placed in the output plane (see Fig. 1) will observe a shifted and decorrelated version of the original field incident on it (due to the effect of the aperture). By examining the magnitude of this shift, information about the motion of the surface at the input plane can be determined.

An imaging system can be described as a convolution of the FT of the system's limiting pupil function (its unsealed impulse response) with the ideal image predicted by using geometrical optics.[4,36] Consider a diffraction-limited 4-f imaging system architecture where the aperture is in the Fourier plane. A tilt in the input plane will cause a spatial shift of the distribution at the aperture (Fourier) plane.[37] It is pointed out in Ref. 4 that it is this tilting that leads to a decorrelation in the output plane between the initial field and the field after motion or deformation. A measure of this decorrelation is given by the Yamaguchi correlation factor [see Eq. (11) in Ref. 4]. However, in the optical arrangement that we are considering (and unlike that in a 4-f imaging system), both tilting and in-plane translation of the input surface contribute to a spatial shift of the distribution at the aperture plane and some linear phase term, and thus both effects are responsible for the decorrelation of the two fields in the output plane.

So far we expect that there will be decorrelation in the output plane between the initial image and the image captured after motion, primarily due to the aperture in the system. We also expect that if the decorrelation is not total, there should be a cross-correlation peak. The position of this peak relative to that of the auto-correlation peak of the initial image.[19,20] contains information about the motion of the input surface. If the aperture were infinite in extent, then a direct LCT-based analysis could pre-

dict the location of this cross-correlation peak. A finite aperture in the system means that we are no longer dealing with a lossless shift invariant system; however, if the relationship between the input and output coordinate systems is partially preserved, despite the presence of an aperture, then an LCT-based analysis may still prove useful. Ideally we would like to derive an expression that can (i) quantify the expected decorrelation due to the aperture, i.e., a generalized Yamaguchi correlation factor and (ii) also predict the location of the cross-correlation peak. We continue with a 1-D analysis. Let the aperture be described by the function $p(\cdot)$. The undeformed and deformed fields (see Fig. 1) immediately after the aperture, $v_a(\cdot)$ and $\tilde{v}_a(\cdot)$, are then given by

$$v_a(\cdot) = u_a(\cdot)p(\cdot) \quad \tilde{v}_a(\cdot) = \tilde{u}_a(\cdot)p(\cdot). \tag{4}$$

The field incident on the camera before motion can be written as

$$v_c(x_c) = \int v_a(x_a)\exp\left[\frac{j\pi}{\lambda B_2}(D_2x_c^2 + A_2x_a^2 - 2x_ax_c)\right]\mathrm{d}x_a. \tag{5}$$

The field incident on the camera after motion, $\tilde{v}_c(x_c)$, is defined in a similar manner. Following the approach taken in Ref. 4, we write the normalized covariance $c_{I\tilde{I}}(s)$ as

$$c_{I\tilde{I}}(s) = \frac{|\langle v_c^*(r)\tilde{v}_c(r+s)\rangle|^2}{\sigma_I\sigma_{\tilde{I}}}, \tag{6}$$

where σ_ψ is the variance defined as $\sigma_\psi^2 = \langle\psi\rangle^2 - \langle\psi^2\rangle$ (see Ref. 4), the angled brackets $\langle\ \rangle$ denote ensemble average, and * denotes the complex conjugate. The numerator in Eq. (6) is given by

$$\begin{aligned}\langle v_c^*(x_c)\tilde{v}_c(x_c+s)\rangle = \int\int \langle u_a^*(x_a)\tilde{u}_a(\tilde{x}_a)\rangle p^*(x_a)p(\tilde{x}_a) \\ \times\exp\left[\frac{-j\pi}{\lambda B_2}(D_2x_c^2 + A_2x_a^2 - 2x_ax_c)\right] \\ \times\exp\left\{\frac{j\pi}{\lambda B_2}\left[D_2(x_c+s)^2 + A_2\tilde{x}_a^2 - 2\tilde{x}_a(x_c\right.\right. \\ \left.\left. + s)\right]\right\}\mathrm{d}x_a\mathrm{d}\tilde{x}_a.\end{aligned} \tag{7}$$

The term $\langle u_a^*(x_a)\tilde{u}_a(\tilde{x}_a)\rangle$ is given by

$$\begin{aligned}\langle u_a^*(x_a)\tilde{u}_a(\tilde{x}_c)\rangle = \int\int \langle u^*(x_0)\tilde{u}(\tilde{x}_0)\rangle\exp\left[\frac{-j\pi}{\lambda B_1}(D_1x_a^2 + A_1x_0^2\right. \\ \left. - 2x_ax_0)\right]\exp\left[\frac{j\pi}{\lambda B_1}(D_1\tilde{x}_a^2 + A_1\tilde{x}_0^2\right. \\ \left. - 2\tilde{x}_a\tilde{x}_0)\right]\mathrm{d}x_0\mathrm{d}\tilde{x}_0.\end{aligned} \tag{8}$$

We assume that the coherence area of the speckle field at the scattering plane is very small compared with the size of the illuminated region and can be approximated by a delta function.[4,8,10,38] Thus using Eq. (1) to describe $\tilde{u}(\tilde{x}_0)$, we write

$$\begin{aligned}\langle u^*(x_0)\tilde{u}(\tilde{x}_0)\rangle &= \left\langle u^*(x_0)u(x_0+\xi)\exp\left(j\frac{2\pi}{\lambda}\kappa x_0\right)\right\rangle \\ &= \sigma_u^2\delta(\tilde{x}_0 - x_0 - \xi)\exp\left(j\frac{2\pi}{\lambda}\kappa\tilde{x}_0\right).\end{aligned} \tag{9}$$

Substituting Eq. (9) into Eq. (8), we get that

$$\begin{aligned}\langle u_a^*(x_a)\tilde{u}_a(\tilde{x}_a)\rangle = \sigma_u^2\int\exp\left[\frac{-j\pi}{\lambda B_1}(D_1x_a^2 + A_1x_0^2 - 2x_ax_0)\right] \\ \times\exp\left[j\frac{2\pi}{\lambda}\kappa(x_0+\xi)\right]\exp\left\{\frac{j\pi}{\lambda B_1}\left[D_1\tilde{x}_a^2\right.\right. \\ \left.\left. + A_1(x_0+\xi)^2 - 2\tilde{x}_a(x_0+\xi)\right]\right\}\mathrm{d}x_0.\end{aligned} \tag{10}$$

Simplifying Eq. (10) give

$$\begin{aligned}\langle u_a^*(x_a)\tilde{u}_a(\tilde{x}_a)\rangle = \sigma_u^2\exp\left\{\frac{j\pi}{\lambda B_1}\left[D_1(\tilde{x}_a^2 - x_a^2) - 2\tilde{x}_a\xi\right]\right\} \\ \times\int\exp\left(\frac{-j\pi 2x_0\Delta}{\lambda B_1}\right)\mathrm{d}x_0,\end{aligned} \tag{11}$$

where $\Delta = \tilde{x}_a - (x_a + A_1\xi + B_1\kappa)$.

The result of calculating the integral, as written in Eq. (11), is $\delta(\Delta)$. This result is correct if we integrate over an infinite input plane x_0, although in practice we integrate only over the finite area of the optically rough surface that is illuminated. Limiting the region of integration acts to "smear" or broaden the $\delta(\Delta)$ function.[37] If we assume that the correlation area [which is the broadened $\delta(\Delta)$ function] is very small compared with the area of the scattering plane (region of integration) and of the aperture plane (see in particular Subsections 5.6, 7.2, and 7.5 of Ref. 38), the integral in Eq. (11) is a narrow function that we approximate by $C\delta(\Delta)$, where C is an unimportant constant. Thus we substitute Eq. (11) into Eq. (7) to get

$$\begin{aligned}\langle v_c^*(x_c)\tilde{v}_c(x_c+s)\rangle = C\sigma_u^2\int\int \delta(\tilde{x}_a - x_a - A_1\xi - B_1\kappa) \\ \times\exp\left\{\frac{j\pi}{\lambda B_1}\left[D_1(\tilde{x}_a^2 - x_a^2)\right.\right. \\ \left.\left. - 2\tilde{x}_a\xi\right]\right\}p^*(x_a)p(\tilde{x}_a)\exp\left\{\frac{j\pi}{\lambda B_2}\left[D_2(s^2\right.\right. \\ \left. + 2sx_c) + A_2(\tilde{x}_a^2 - x_a^2) - 2x_c(\tilde{x}_a - x_a)\right. \\ \left.\left. - 2s\tilde{x}_a\right]\right\}\mathrm{d}x_a\mathrm{d}\tilde{x}_a.\end{aligned} \tag{12}$$

Integrating with respect to $\mathrm{d}\tilde{x}_a$, we get

$$\langle v_c^*(x_c)\tilde{v}_c(x_c+s)\rangle = C\sigma_u^2 \int \exp\left\{\frac{j\pi}{\lambda B_1}[2D_1(A_1\xi+B_1\kappa)x_a - 2x_a\xi]\right\} p^*(x_a)p(x_a+A_1\xi+B_1\kappa) \times \exp\left\{\frac{j\pi}{\lambda B_2}[D_2(s^2+2sx_c)+2A_2(A_1\xi+B_1\kappa)x_a - 2x_c(A_1\xi+B_1\kappa) - 2s(x_a+A_1\xi+B_1\kappa)]\right\} dx_a. \quad (13)$$

The magnitude is given by

$$|\langle v_c^*(x_c)\tilde{v}_c(x_c+s)\rangle| = \left| C\sigma_u^2 \int p^*(x_a)p(x_a+A_1\xi+B_1\kappa) \times \exp\left(\frac{j\pi}{\lambda}\left\{\frac{[2D_1(A_1\xi+B_1\kappa)-2\xi]}{B_1} + \frac{[2A_2(A_1\xi+B_1\kappa)-2s]}{B_2}\right\}x_a\right) dx_a \right|. \quad (14)$$

By the Schwartz inequality[39] and noting that $A_1D_1 - B_1C_1 = 1$,

$$|\langle v_c^*(x_c)\tilde{v}_c(x_c+s)\rangle|^2 \leq \sigma_u^4 C^2 \left| \int p^*(x_a)p(x_a+A_1\xi+B_1\kappa)dx_a \right|^2, \quad (15)$$

and therefore Eq. (14) has a maximum value when

$$s = [A_1A_2 + B_2C_1]\xi + [A_2B_1 + B_2D_1]\kappa. \quad (16)$$

Thus the shift of the distribution in the output plane is specifically related to the bulk optical system and the in-plane translation and tilting of the surface.

By a similar analysis we find that

$$|\langle v_a^*(x_a)v_a(x_a)\rangle|^2 \leq C\sigma_u^2 \int |p(x_a)|^2 dx_a,$$

$$|\langle \tilde{v}_a^*(x_a)\tilde{v}_a(x_a)\rangle|^2 \leq C\sigma_u^2 \int |p(x_a)|^2 dx_a. \quad (17)$$

Thus the maximum value of Eq. (13) occurs when

$$C_{\tilde{II}} = \left| \frac{\int p^*(x_a)p(x_a+A_1\xi+B_1\kappa)dx_a}{\int |p(x_a)|^2 dx_a} \right|^2. \quad (18)$$

This equation specifically gives the expected decorrelation in the output plane for a given system. It is dependent on the first LCT system (see Fig. 1) only and on the autocorrelation of the aperture function (see Fig. 1) and as such can be considered the generalized Yamaguchi correlation factor.

Based on these results we note three points:

1. The maximum correlation peak in the output coordinate system occurs when $s=[A_1A_2+B_2C_1]\xi+[A_2B_1+B_2D_1]\kappa$. The simpler LCT-based analysis predicts exactly the same shift in the output distribution, indicating that it still provides a useful means for interpreting and designing metrology systems.[40]

2. We have also derived a decorrelation term, Eq. (18), equivalent to a general Yamaguchi correlation factor. Unlike the Yamaguchi correlation factor, as defined by Eq. (11) in Ref. 4, our generalized correlation factor is not dependent solely on tilt κ but also on the ξ_a term, where $\xi_a = A_1\xi + B_1\kappa$, which is dependent on both the in-plane translation ξ and the tilting κ of the input surface.

3. In the special case of an imaging metrology system, where the limiting aperture is located in the Fourier plane, the parameters for LCT system 1 (see Fig. 1) are given by $\{A_1,B_1,C_1,D_1\}=\{0,1/q,-q,0\}$ [see Eq. (2c)], where q is some scaling factor. This results in a decorrelation factor that is dependent solely on the tilting ($A_1=0$) of the rough surface, and thus our results are consistent with the analysis presented in Ref. 4.

B. Design and Optimization of Metrology Systems Using the Linear Canonical Transform

In this subsection we would like to demonstrate the flexibility of an LCT approach to the design of metrology systems. Central to the flexibility of the LCT is the fact that it can describe many different QPS optical systems and that even more complex systems can derived by cascading successive LCT systems together[33]:

$$\begin{bmatrix} 0 & f \\ -1/f & 0 \end{bmatrix}, \quad \begin{bmatrix} \cos(\theta) & f\sin(\theta) \\ -\sin(\theta)/f & \cos(\theta) \end{bmatrix}, \quad \begin{bmatrix} 1 & z \\ 0 & 1 \end{bmatrix}, \quad \begin{bmatrix} 1 & 0 \\ -1/f & 1 \end{bmatrix}. \quad (19)$$

In Eqs. (19) we provide the *ABCD* matrix representations for some of the well-known optical systems. These four systems are the OFT, OFRT, FST and CMT, respectively, where θ in the second matrix refers to the fractional angle of the OFRT system, z is the distance of free-space propagation (FST), and f corresponds to the focal length of the thin lens (CMT). For completeness we note in passing that a more general linear transform exists that includes fixed position or phase shifts and is able to describe offsets with respect to the optical axis as well as the effects of gratings and prisms.[41–43]

The effect of successive LCTs is given by appropriately combining the matrices of the individual LCTs[33] together. To give a practical example, consider the two-lens optical system depicted in Fig. 2. Using the appropriate matrices from Eqs. (19) (only FST and CMT matrices are used) to model the passage of light from input plane to output plane, we can derive the *ABCD* matrix for the whole system:

$$\begin{bmatrix} A & B \\ C & D \end{bmatrix} = \begin{bmatrix} 1 & d_3 \\ 0 & 1 \end{bmatrix} \begin{bmatrix} 1 & 0 \\ -1/f_2 & 1 \end{bmatrix} \begin{bmatrix} 1 & d_2 \\ 0 & 1 \end{bmatrix} \begin{bmatrix} 1 & 0 \\ -1/f_1 & 1 \end{bmatrix} \begin{bmatrix} 1 & d_1 \\ 0 & 1 \end{bmatrix}$$
$$= \begin{bmatrix} 1 - \dfrac{d_3 + d_2(1 - d_3/f_2)}{f_1} - \dfrac{d_3}{f_2} & d_3 + d_2 + \dfrac{d_1 d_2 d_3 - (d_1 + d_2) d_3 f_1 - (d_2 + d_3 - f_1) d_1 f_2}{f_1 f_2} \\ \dfrac{d_2/f_2 - 1}{f_1} - \dfrac{1}{f_2} & 1 + d_1\left(\dfrac{d_2/f_2 - 1}{f_1} - \dfrac{1}{f_2}\right) - \dfrac{d_2}{f_2} \end{bmatrix}. \quad (20)$$

Examining Eq. (20), we see that if we set $d_1=f_1$, $d_3=f_2$, and $d_2=d_1+d_3$, then we get $\{A,B,C,D\}=\{-f_2/f_1, 0, 0, f_2/f_1\}$. This happens to be a 4-f imaging system with a magnification given by $-f_2/f_1$, which is insensitive to tilting motion since $B=0$. Alternatively setting $f_1=f_2=f$, $d_1=d_3=2f$, and $d_2=3f$, we have the OFT system $\{0, -f, 1/f, 0\}$. This system is insensitive to in-plane translation, since $A=0$.

Using this two-lens optical system, we can build scale invariant OFRT systems.[28] In this case the *ABCD* matrix is as in Eqs. (19) with $A=\cos(\theta)$ and $B=f\sin(\theta)$. This type of system is thus sensitive to both tilting and in-plane translation motion. By varying the fractional order of the OFRT system,[19,20] the sensitivity of the system can be changed. Clearly the A and B parameters of an OFRT system have absolute maximum values of unity and f, respectively, which limits the flexibility of the system. As noted in Ref. 28, implementing an OFRT system imposes restrictions on the possible values for d_1, d_2, etc. Relaxing these conditions realizes an LCT system that has a much larger range of A and B parameter values, making it more flexible than the previous optical systems. This is illustrated in Fig. 2(a) in Ref. 40, where $-5<A<2.5$ for $\{d_1=5\text{ cm}, \quad 0<d_2<50\text{ cm}, \quad 0<d_3<50\text{ cm}, \quad f_1=20\text{ cm}, \quad f_2=10\text{ cm}\}$ and in Fig. 2(b) in Ref. 40, where $-10<B<0$ for $\{0<d_1<50\text{ cm}, \quad 0<d_2<50\text{ cm}, \quad d_3=10\text{ cm}, \quad f_1=5\text{ cm}, \quad f_2=10\text{ cm}\}$.

Before closing this subsection, we add that using this type of design approach in conjunction with the generalized Yamaguchi correlation factor, Eq. (18), allows optimization of the metrology system for measurement of a particular parameter. Suppose that we want to design an OFT system for measuring small surface tilting. Let us choose the two-lens OFT system above with $f_1=f_2=f$, $d_1=d_3=2f$, and $d_2=3f$, which gives the overall system matrix of $ABCD=\{0, -f, 1/f, 0\}$. What is the optimum location for the aperture plane in this system so that the generalized Yamaguchi correlation factor is a maximum?

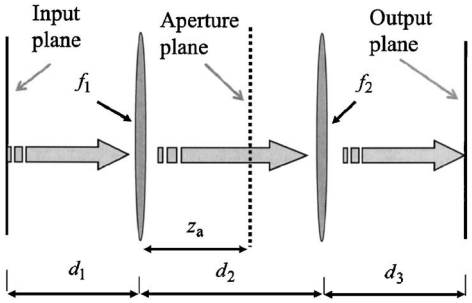

Fig. 2. Two-lens optical LCT system with an aperture plane.

Referring back to Fig. 1, we now decompose this OFT system into two separate matrices, the first matrix, M_1, describing propagation from the input plane to the aperture plane and the second from the aperture plane to the camera plane. By placing the aperture a distance z_a after the first lens in Fig. 2, we have

$$M_1 = \begin{bmatrix} 1 - \dfrac{z_a}{f} & 2f\left(1 - \dfrac{z_a}{f}\right) + z_a \\ -\dfrac{1}{f} & -1 \end{bmatrix}. \quad (21)$$

Since we are trying to minimize the decorrelation in the output plane due to tilting of the surface, we want to minimize the B element of M_1 in Eq. (21). Setting this B element to zero gives $z_a=2f$, so the aperture ideally should be located two focal lengths from the first lens (see Fig. 2). In this optical system there will be no decorrelation due to the aperture for tilting motion. There are several other potential sources of decorrelation, one of which is the finite extent of the camera.[19]

C. Illuminating with Fields of Varying Curvature

In this subsection we would like to describe how the reflected field from an optically rough surface varies as the illuminating field is changed from a plane wave to a wave field with a quadratic curvature, i.e., an ideal (in the paraxial regime) converging or diverging spherical wave. For simplicity and brevity we continue with a 1-D analysis and start by assuming plane wave illumination. The field, just after reflection from the optically rough surface, can be described by

$$u(x_0) = \exp[jkh(x_0)], \quad (22)$$

where $k=2\pi/\lambda$, and $h(x_0)$ accounts for the random phase accumulated by the plane wave on reflection from the rough surface.

Changing the illumination field to a converging or diverging spherical wave, the illuminating field can be described, using a quadratic phase approximation, by

$$u_{\text{sph}}(x,z) = \exp\left[\frac{-jkx^2}{2(\varepsilon - z)}\right], \quad (23)$$

where we have omitted an intensity scaling factor $\sqrt{(\varepsilon - z)/z}$. Such a spherical wave field may be produced by placing a lens in the path of the illuminating plane wave at a distance $z=z_{\text{RS}}$ from the rough surface (see Fig. 3), in which case $\varepsilon=f$, the focal length of the illuminating lens.

After reflection from the optically rough surface this converging (or diverging) spherical wavefront is altered and can, in the paraxial case, be approximated by $u_{sw}(x_0)$, where

$$u_{sw}(x_0) = \exp\left\{jk\left[\frac{-x_0^2}{2(f-z_{RS})} + h(x_0)\right]\right\} = u(x_0)\exp\left[\frac{-j\pi x_0^2}{\lambda(f-z_{RS})}\right]. \quad (24)$$

Equation (24) assumes that the random phase accumulated due to the surface roughness is independent of the phase of the incident wave field. The assumption has been justified by experimental results.[40] The metrology system described using the matrix $\{A,B,C,D\}$ now operates on this reflected speckle field. The resultant field, $v_{sw}(X_{c1})$, incident on the CCD in the output plane is given by

$$v_{sw}(x_{c1}) = \int_{-\infty}^{\infty} u_{sw}(x_0)\exp\left[\frac{j\pi}{\lambda B}(Ax_0^2 + Dx_{c1}^2 - 2x_{c1}x_0)\right]dx_0, \quad (25)$$

which can be rewritten as

$$v_{sw}(x_{c2}) = \int_{-\infty}^{\infty} u(x_0)\exp\left[\frac{j\pi}{\lambda B_{sw}}(A_{sw}x_{c2}^2 + D_{sw}x_0^2 - 2x_{c2}x_0)\right]dx_0, \quad (26)$$

where $B_{sw}=B$, $D_{sw}=D$, and $A_{sw}=A-B/(f-z_{RS})$. By replacing the field $u_{sw}(x)$ in Eq. (25) with $u(x)$ and changing the *ABCD* parameters accordingly, we see that $u(x)$ has effectively been transformed into a different LCT domain (x_{c2}) in the camera plane.

This result can also be derived by using the *ABCD* matrix notation. Noting that $u_{sw}(x_0)$ can be written as $u(x_0)$ multiplied by a quadratic phase factor, or CMT as defined in Eq. (24), we can write

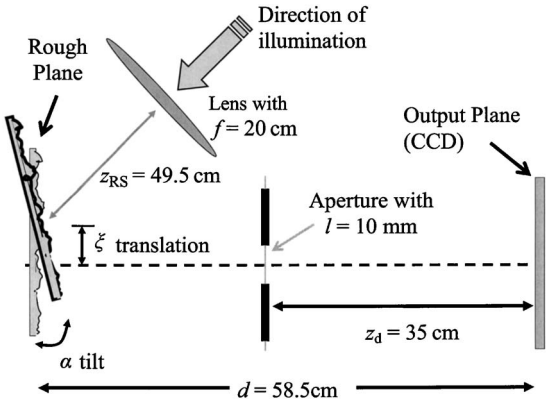

Fig. 3. Experimental setup.

$$\begin{bmatrix} A_{sw} & B_{sw} \\ C_{sw} & D_{sw} \end{bmatrix} = \begin{bmatrix} A & B \\ C & D \end{bmatrix}\begin{bmatrix} 1 & 0 \\ -1/(f-z_{RS}) & 1 \end{bmatrix} = \begin{bmatrix} A - \dfrac{B}{f-z_{RS}} & B \\ C - \dfrac{D}{f-z_{RS}} & D \end{bmatrix} \quad (27)$$

We further note that B_{sw} is equal to B, and thus variation of the curvature of the illuminating field has no effect on the measurement of small surface tilting of the optically rough surface. To estimate the output tilting and in-plane translation motion, we then solve two simultaneous equations,[18–20] giving

$$\xi = \frac{\xi_{c1} - \xi_{c2}}{A - A_{sw}}, \quad \kappa = \frac{A_{sw}\xi_{c1} - A\xi_{c2}}{B(A_{sw} - A)}, \quad (28)$$

where A is the system parameter under plane wave illumination, A_{sw} is the system parameter under spherical wave illumination, $B=B_{sw}$, and the two corresponding motions in the camera plane are ξ_{c1} and ξ_{c2}, respectively.

3. EXPERIMENTAL RESULTS

This section is divided into five subsections. In Subsection 3.A we briefly describe the experimental setup, then in Subsection 3.B we discuss the aperture diameter, the resulting speckle size, and its implications for our experiments. In Subsections 3.C and 3.D we present experimental results for the estimation of in-plane translation and small surface tilts, respectively, illuminating with fields of two different curvatures, namely a diverging spherical wave and a plane wave. In Subsection 3.E we experimentally demonstrate that we can measure both tilt and translation motion simultaneously provided that the motion is captured under at least two different illuminating conditions (in two domains).

A. Experimental Setup

An LCT system (as depicted in Fig. 3) was implemented with a rough surface (4 cm by 8 cm rectangular piece of aluminum) located a distance $d=58.5$ cm from the face of the CCD camera. There is an aperture with a diameter of 10 mm in the LCT system, located at $z_d=35$ cm from the CCD. The curvature of the illuminating field was varied by placing a converging focal lens (see Fig. 3), with $f=20$ cm, in the collimated illumination beam at a distance $z_{RS}=49.5$ cm from the rough target. Thus when the lens is in place, a diverging beam is incident on the surface, and when the lens is removed, we revert to plane wave illumination. The target is illuminated at an angle of 15° by an argon-ion laser with $\lambda=488$ nm. The parameters for the two optical systems (plane wave and diverging spherical wave illumination) are $\{A,B,C,D\}=\{1,0.585,0,1\}$ and $\{A_{sw},B_{sw},C_{sw},D_{sw}=\{2.983,0.585,3.389,1\}$, respectively. The CCD used was a Sony XC ES50CE,[44] which has a pixel size of 8.6 μm $\times$ 8.3 μm, a sensing area of 6.5 mm $\times$ 4.8 mm, and uses no additional imaging optics. After image acquisition the size of the grabbed image was 450 $\times$ 410 pixels. The auto-correlation and cross correlation of

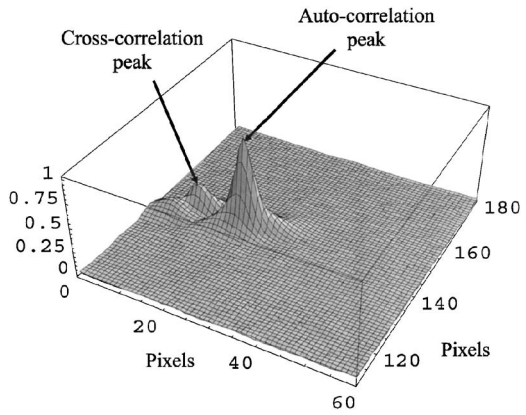

Fig. 4. Correlation results for translation of 100 μm for an LCT system with plane wave illumination. Measured displacement, 99.96 μm.

the images were implemented by using the MATLAB function normxcorr2.[45] This produces quite a large correlation matrix (900×820 pixels). Because of this we display only the relevant section of the correlation matrix in our experimental plots, with the result that sometimes the autocorrelation peak is not in the center of the figure. The surface was translated by using a translation stage driven by an Oriel Encoder Mike actuator, controlled with the 18113 Oriel Mike Control System. The motion stage is rated to have a positional resolution of 0.1 μm. However, it was found that the stage could be positioned with an accuracy of $\sim \pm 1$ μm.[19,20] A similar translation stage is used to drive the rotation stage, where a translation of 161 μm corresponds to 1° of rotation. This allows the optically rough surface to be rotated with an error in angular position of 0.1 mrad.

The aim of our experimental section is to demonstrate the effectiveness of an LCT-based approach to design, not to produce a fully optimized metrology system. As a result we would like to highlight the limitations in the system as it is. We do not for example use interpolation schemes with our grabbed images to achieve subpixel accuracy, with the result that the smallest shift of the distribution in the CCD plane that we can detect is equal to the camera pixel size of ~ 8.3 μm.[44] Also, since we are interested only in the location of the cross-correlation peak, we use the normxcorr2 function from MATLAB,[45] as opposed to the more effective covariance scheme for detecting and emphasizing these peaks as outlined in Chapter 2 of Ref. 6.

B. Lateral Speckle Size

The lateral speckle size (for a circular scattering area) can be calculated by using the formula $1.22\lambda(z_d/l)$.[8,10] The wave field incident on the rough target forms an approximately circular illumination spot with a diameter of 10 cm, so in the aperture plane we calculate a speckle size of approximately 1.4 μm.[8,10] The aperture diameter is 10 mm. Since the aperture area is thus very large compared with the coherence area of the speckle field,this justifies the assumption made in Eqs. (11) and (12) that since the width of the $\langle u_a^*(x_a)\tilde{u}_a(\tilde{x}_a)\rangle$ function is "sufficiently narrow to keep the other functions in the integrand constant within the width," then $\langle u_a^*(x_a)\tilde{u}_a(\tilde{x}_a)\rangle$ may be expressed as a delta function.[46] Since there are approximately 5×10^7 individual speckles within the aperture area with random phase and amplitude, we can consider this plane to be the effective scattering plane for the metrology system. This results in a lateral speckle size in the camera plane of ~ 21 μm.

C. In-Plane Translation Results

The target was initially illuminated with a plane wave, an image of the reflected speckle field was captured, the target was then moved, and another image of the (now modified) speckle field was also captured. To determine the motion of the target, the two images were correlated, allowing both the magnitude and direction of the motion to be determined.[19,20] The result is displayed in Fig. 4, and two peaks are clearly visible in the plot. The first peak, with a magnitude of unity, is the normalized autocorrelation of the first grabbed image with itself and serves as the origin. The second and smaller peak is the cross correlation of the first and second images. The direction is determined by noting to which side of the autocorrelation peak this secondary peak is positioned. It is possible to estimate the magnitude of the motion by determining the separation of the two peaks. In this case the actual motion moved was 100 μm, and the measured motion was 99.96 μm. As noted, the size of the secondary peak (0.3271) is smaller than the auto-correlation, indicating that decorrelation between the two captured images has occurred.

The target was then illuminated with a diverging spherical beam. The spherical beam was produced by placing the converging lens of focal length of a collimated plane wave a distance of 49.5 cm from the target (see Fig. 3). Using the same procedure to grab and process the captured images and employing Eq. (16), the target, which was again translated a distance of 100 μm but in the opposite direction to that before, was estimated to have moved 100.5 μm. The results have been plotted in Fig. 5. Again the secondary peak is smaller (0.5325) than the auto-correlation peak, indicating that there is decorrelation. We draw the reader's attention to the location of the secondary peak with respect to the auto-correlation peak in Fig. 5. From this we can infer that the target has been moved in the direction opposite to that in Fig. 4.

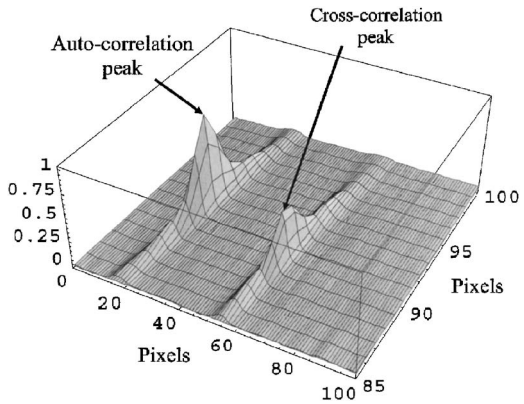

Fig. 5. Correlation results for translation of 100 μm for an LCT system with diverging wave illumination. Measured displacement, 100.5 μm.

From Eq. (20) it is expected that the metrology system's sensitivity to in-plane translation motion should be changed as the curvature of the illuminating field is varied. Examining Figs. 4 and 5, it is clear that the sensitivity of the system has been altered, as the separation between the auto-correlation peak and secondary peak in Fig. 5 is greater than that in Fig. 4 even though the rough target has been translated by the same amount on both occasions. There appears to be an asymmetry in the peaks displayed in Figs. 4 and 5; however, this is due simply to the different x- and y-axis scales in the plots. Indeed this is also true of later figures.

D. Small Surface Tilting Results

Again the target was illuminated by a plane wave under the same conditions as those in Subsection 3.A. The rough target was tilted through a small angle $\alpha = 0.54$ mrad, and the estimated motion was ~ 0.53 mrad. The results are plotted in Fig. 6. The separation between the two peaks is quite large in comparison with the in-plane translation results (see Figs. 4 and 5), indicating that quite small angles can be easily measured.[11] The secondary peak is, as expected, smaller than the autocorrelation peak, with a value of 0.6506.

E. Simultaneous Tilt and Translation Measurement

The optically rough target was moved by a small angle $\alpha = 0.54$ mrad and translated by 50 μm, this motion was captured under the two different illuminating conditions (plane and diverging spherical), and the grabbed images were processed. The result is plotted in Fig. 7. Our model predicts that the diverging wave illumination will cause a larger translation in the output plane, since the A parameter for this system is larger (see Subsection 3.A), and this is evident in Fig. 7. Using Eqs. (28), the estimated translation was 46.2 μm while the estimated rotation was an exact 0.54 mrad. The combination of Eqs. (28) and the chosen LCT system parameters means that the estimation of the in-plane translation is sensitive to error. By choosing a different value for A_{sw}, it should be possible to make this metrology system more robust to in-plane translation measurement.

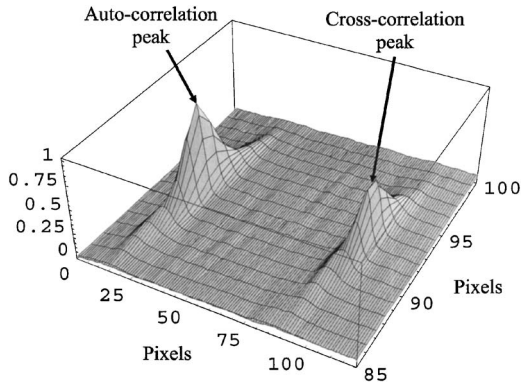

Fig. 6. Correlation results for rotation of 0.55 mrad for an LCT system where the target is illuminated with a plane wave. Measured rotation, 0.534 mrad.

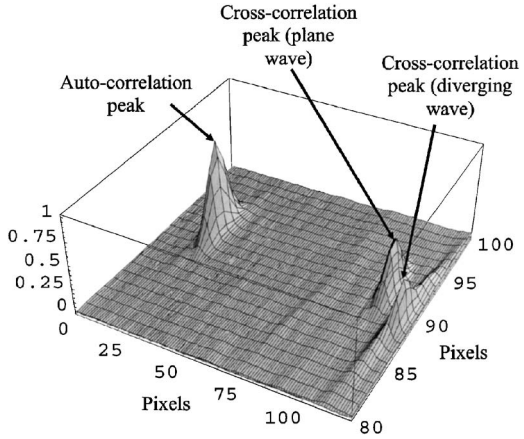

Fig. 7. Correlation results for simultaneous in-plane translation of 50 μm and rotation of 0.55 mrad. Measured rotation, 0.55 mrad; in-plane translation, 46.1 μm.

4. CONCLUSIONS

We have shown that an optical system modeled by using a linear canonical transform (LCT) can be used to vary the range and sensitivity of a speckle-based metrology system. Using compact *ABCD* matrix notation,[33] the metrology system's sensitivity to both in-plane translation and to tilting motion was related specifically to bulk optical elements present in the system; i.e., any number of lenses and free-space propagation distances could be accounted for. It was also noted[18–20,34] that the magnitude and direction of both in-plane translation and tilting motion of an optically rough target can be discerned if that motion is captured in two separate LCT domains. In Subsection 2.A we showed that an LCT-based analysis is useful in designing and interpreting general metrology systems despite the fact that the presence of a finite aperture violates the lossless condition assumed when using the LCT analysis.

A generalized form of the Yamaguchi correlation factor was derived that explicitly relates the decorrelation between images, captured before and after motion, to both in-plane translation and tilting of the optically rough input surface. In our derivation the rough surface was assumed to remain constant, i.e., there were no changes in the surface microstructure and the surface was unaffected by environmental factors such as the presence of condensation, as considered by other authors.[4,6]

It has been shown that in the paraxial approximation illuminating a target with wavefronts of different curvature can be used to effectively change the LCT domain. In Subsection 2.C we derived expressions, which include the illuminating field curvature with the *ABCD* matrix parameters that define the LCT system. By capturing the output intensity from an optically rough target, illuminated by two fields of different curvature, both the direction and magnitude of the rigid body's motion (tilting and in-plane translation) can be unambiguously determined.

In Section 3 we experimentally demonstrated our ability to accurately measure in-plane translation motion by using illuminating fields of different curvature. It has been shown that the sensitivity of the metrology system can be related to the curvature of the illuminating field.

Much remains to be done, including a detailed experimental verification of our proposed generalized Yamaguchi correlation factor.[47] To achieve this, the covariance algorithm described in Ref. 6 must be implemented so that precise calculation of the expected decorrelation is possible. In fact, in Refs. 4 and 6 the amount of decorrelation is used as a means to estimate the magnitude of tilts, allowing measurement of translation and tilt simultaneously by using a single imaging system.

Furthermore, in the analysis of the quadratic phase systems described here, i.e., LCT systems 1 and 2 (see Fig. 1), the finite extents of the lens apertures are not explicitly considered.[48] Others have approached this problem by using complex *ABCD* notation, assuming Gaussian apodized apertures.[49,50] Clearly much also remains to be done in this area.

ACKNOWLEDGMENTS

We acknowledge the support of Enterprise Ireland and Science Foundation of Ireland through the Research Innovation Fund, the Basic Research Programme, and the Research Frontiers Programme. We also acknowledge the support of the Irish Research Council for Science, Engineering and Technology.

Corresponding author: John T. Sheridan; e-mail: john.sheridan@ucd.ie; tel: +353-(0)1-7716-1927; fax: +353-(0)1-283-0921; website, http://www.ucd.ie/eleceng.

REFERENCES

1. J. W. Goodman, "Statistical properties of laser speckle patterns," in *Laser Speckle and Related Phenomena*, J. C. Dainty, ed. (Springer-Verlag, 1975).
2. R. Jones and C. Wykes, *Holographic and Speckle Interferometry* (Cambridge U. Press, 1989).
3. J. C. Dainty, "The statistics of speckle patterns," in *Progress in Optics, Vol. XIV*, E. Wolf, ed. (North-Holland, 1976).
4. T. Fricke-Begemann, "Three-dimensional deformation field measurement with digital speckle correlation," Appl. Opt. **42**, 6783–6796 (2003).
5. T. Fricke-Begemann, "Speckle interferometry: three-dimensional deformation field measurement with a single interferogram," Appl. Opt. **40**, 5011–5022 (2001).
6. T. Fricke-Begemann, "Optical measurement of deformation fields and surface processes with digital speckle correlation," Ph.D. dissertation (Carl von Ossietzky Universität Oldenburg, 2002).
7. M. Owner-Petersen, "Decorrelation and fringe visibility: on the limiting behavior of various electronic speckle-pattern interferometers," J. Opt. Soc. Am. A **8**, 1082–1089 (1991).
8. L. Leushacke and M. Kirchner, "Three-dimensional correlation coefficient of speckle intensity for rectangular and circular apertures," J. Opt. Soc. Am. A **7**, 827–832 (1990).
9. P. Gundu, E. Hack, and P. Rastogi, "Superspeckles: a new application of optical superresolution," Opt. Express **13**, 6468–6475 (2005).
10. Q. Li and F. Chiang, "Three-dimensional dimension of laser speckle," Appl. Opt. **31**, 6287–6291 (1992).
11. H. Tiziani, "A study of the use of laser speckle to measure small tilts of optically rough surfaces accurately," Opt. Commun. **5**, 271–274 (1972).
12. P. K. Rastogi, *Digital Speckle Pattern Interferometry and Related Techniques* (Wiley, 2001).
13. P. K. Rastogi, "Techniques of displacement and deformation measurements in speckle metrology," in *Speckle Metrology*, R. S. Sirohi, ed. (Marcel Dekker, 1993).
14. M. Sjodahl, "Electronic speckle photography: measurement of in-plane strain fields through the use of defocused laser speckle," Appl. Opt. **34**, 5799–5808 (1995).
15. J. M. Diazdelacruz, "Multiwindowed defocused electronic speckle photographic system for tilt measurement," Appl. Opt. **44**, 2250–2257 (2005).
16. J. T. Sheridan and R. Patten, "Fractional Fourier speckle photography: motion detection and the optical fractional Fourier transformation," Optik (Stuttgart) **111**, 329–331 (2000).
17. J. T. Sheridan and R. Patten, "Holographic interferometry and the fractional Fourier transformation," Opt. Lett. **25**, 448–450 (2000).
18. J. T. Sheridan, B. M. Hennelly, and D. Kelly, "Motion detection, the Wigner distribution function, and the optical fractional Fourier transform," Opt. Lett. **28**, 884–886 (2003).
19. D. P. Kelly, B. M. Hennelly, and J. T. Sheridan, "Magnitude and direction of motion with speckle correlation and the optical fractional Fourier transform," Appl. Opt. **44**, 2720–2727 (2005).
20. D. P. Kelly, B. M. Hennelly, and J. T. Sheridan, "Speckle correlation and the fractional Fourier transform," in *Optical Information Systems II*, B Javidi, ed., Proc. SPIE **5557**, 255–266 (2004).
21. M. Ozaktas, Z. Zalevsky, and M. A. Kutay, *The Fractional Fourier Transform with Applications in Optics and Signal Processing* (Wiley, 2001).
22. D. Mendlovic, M. Ozaktas, and A. W. Lohmann, "Graded-index media, Wigner-distribution functions, and the fractional Fourier transform," Appl. Opt. **33**, 6188–6193 (1994).
23. D. Mendlovic and H. M. Ozatkas, "Fractional Fourier transformations and their optical implementations," J. Opt. Soc. Am. A **10**, 1875–1881 (1993).
24. H. M. Ozatkas and D. Mendlovic, "Fractional Fourier transformations and their optical implementations," J. Opt. Soc. Am. A **10**, 2522–2531 (1993).
25. A. W. Lohmann, "Image rotation, Wigner rotation and the fractional Fourier transformation," J. Opt. Soc. Am. A **10**, 2181–2186 (1993).
26. R. G. Dorsch, "Fractional Fourier transform of variable order based on a modular lens system," Appl. Opt. **34**, 6016–6020 (1995).
27. A. W. Lohmann, "A fake zoom lens for fractional Fourier experiments," Opt. Commun. **115**, 427–443 (1995).
28. L. Z. Cai and Y. Q. Wang, "Optical implementation of scale invariant fractional Fourier transform of continuously variable orders with a two-lens system," Opt. Laser Technol. **34**, 249–252 (2002).
29. M. J. Bastians, "Application of the Wigner distribution function in optics," in *The Wigner Distribution—Theory and Applications in Signal Processing*, W. Mecklenbrauker and F. Hlawatsch, eds. (Elsevier Science, 1997), Chap. 7.
30. E. Wigner, "On the quantum correction for thermodynamic equilibrium," Phys. Rev. **40**, 749–759 (1932).
31. J. Widjaja, J. Uozumi, and T. Asakura, "Real-time evaluation of local displacement of objects by means of the Wigner distribution function," J. Opt. (Paris) **23**, 13–18 (1992).
32. T. Alieva, M. J. Bastiaans, and M. L. Calvo, "Fractional transforms in optical information processing," EURASIP J. Appl. Signal Process. **10**, 1498–1519 (2005).
33. S. A. Collins, "Lens system diffraction integral written in terms of matrix optics," J. Opt. Soc. Am. **60**, 1168–1177 (1970).
34. R. F. Patten, B. M. Hennelly, D. P. Kelly, F. T. O'Neill, Y. Liu, and J. T. Sheridan, "Speckle photography: mixed domain fractional Fourier motion detection," Opt. Lett. **31**, 32–34 (2006).
35. B. M. Hennelly and J. T. Sheridan, "Fast numerical algorithms for the linear canonical transform," J. Opt. Soc. Am. A **22**, 928–938 (2005).

36. J. W. Goodman, *Introduction to Fourier Optics*, 3rd ed. (Roberts, 2005).
37. R. N. Bracewell, *The Fourier Transform and Its Applications* (McGraw-Hill, 1965).
38. J. W. Goodman, *Statistical Optics* (Wiley, 1985).
39. E. L. O'Neill, *Introduction to Statistical Optics* (Addison-Wesley, 1962).
40. D. P. Kelly, R. F. Patten, B. M. Hennelly, Y. Liu, J. E. Ward, and J. T. Sheridan, "Linear canonical transforms, and speckle based metrology," in *Recent Developments in Traceable Dimensional Measurements III*, J. E. Decken and G.-S. Peng, eds., Proc. SPIE **5879**, 223–234 (2005).
41. S. Abe and J. T. Sheridan, "Generalization of the fractional Fourier transformation to an arbitrary linear loss-less transformation: an operator approach," J. Phys. A **27**, 4179–4187 (1994).
42. S. Abe and J. T. Sheridan, "Optical operations on wave functions as the Abelian subgroups of the special affine Fourier transformation," Opt. Lett. **19**, 1801–1803 (1994).
43. S. C. Pei and J. J. Ding, "Eigenfunctions of the offset Fourier, fractional Fourier, and linear canonical transforms," J. Opt. Soc. Am. A **20**, 522–532 (2003).
44. www.ni.com/third-party/sony/pdf/XC-ES50ES30.pdf.
45. MATLAB toolbox documentation, www.mathworks.com.
46. I. Yamaguchi, K. Kobayashi, and L. Yaroslavsky, "Measurement of surface roughness by speckle correlation," Opt. Eng. **43**, 2753–2761 (2004).
47. D. P. Kelly, J. E. Ward, U. Gopinathan, B. M. Hennelly, F. T. O'Neill, and J. T. Sheridan, "The generalized Yamaguchi correlation factor for quadratic phase speckle metrology systems with apertures," Opt. Lett. (to be published).
48. D. P. Kelly, B. M. Hennelly, W. T. Rhodes, and J. T. Sheridan, "Analytical and numerical analysis of linear optical systems," Opt. Eng. (to be published).
49. H. T. Yura and S. G. Hanson, "Optical beam propagation through complex optical systems," J. Opt. Soc. Am. A **4**, 1931–1948 (1987).
50. H. T. Yura, B. Rose, and S. G. Hanson, "Dynamic laser speckle in complex *ABCD* optical systems," J. Opt. Soc. Am. A **15**, 1160–1166 (1998).